Coplanar lidar measurement of a single wind energy converter wake in distinct atmospheric stability regimes at the Perdigão 2017 experiment

IOP Conf. Series: Journal of Physics: Conf. Series **1037** (2018) 052006 doi:10.1088/1742-6596/1037/5/052006

Coplanar lidar measurement of a single wind energy converter wake in distinct atmospheric stability regimes at the Perdigão 2017 experiment

Norman Wildmann, Stephan Kigle and Thomas Gerz

Institute of Atmospheric Physics, Deutsches Zentrum für Luft- und Raumfahrt e.V., Oberpfaffenhofen, Germany

E-mail: norman.wildmann@dlr.de

Abstract. The understanding of wakes of wind energy converters (WEC) is highly relevant to wind-energy research. In orographically complex terrain, wind is amplified at ridges but also varies significantly, exhibiting strong gustiness and enhanced turbulence levels compared to wind conditions in flat terrain. In this study, long-range lidar instruments are used to detect and analyse the wake of a single WEC in complex terrain in different atmospheric stability regimes. The special orography of two parallel mountain ridges at the Perdigão 2017 experiment allowed to place two lidars in a coplanar set-up and retrieve horizontal as well as vertical wind speed in a cross-section of the terrain which is in-plane with the WEC. In cases of main wind direction, which is parallel to the lidar scans, the wake's propagation can thus be measured far downstream in the valley. A wake tracking algorithm is proposed to automatically detect the wake center in the lidar scans for three periods with distinct atmospheric stability conditions. Wind speed deficits and wake propagation paths are quantified and categorized accordingly. A careful uncertainty estimation is done for the coplanar wind retrieval.

1. Introduction

Wakes of wind energy converters (WEC) are highly dynamic, local features in the atmospheric boundary layer (ABL). The understanding of their interaction with the turbulent background wind field is challenging, especially in complex terrain. Equally challenging is the adequate measurement of wake properties. A better description of the wind velocity deficit that is caused by the wake, its width and propagation path has been the goal of the development of several wake models [1]. Such models are for example used for the siting of multiple wind turbines in limited areas as well as energy yield and fatique load prediction of single wind turbines and whole wind farms. In order to optimize the yield of a wind farm, current studies have successfully shown the possibilities to steer wakes in an optimal way by misaligning the WEC yaw angle with respect to the main wind direction to increase wind farm power output [2]. The most promising tool to gain better understanding of the physics of wakes at the present state-of-the-art are numerical large-eddy simulations (LES) [3, 4, 5, 6, 7]. These simulations can reproduce realistic atmospheric flows and wind turbine wakes, but need validation by real-world experiments. In recent years, lidars have become the measurement systems of choice for wake investigations because of the scales they are able to resolve and their flexible deployment, in particular with scanning systems. For short-distance measurements of the near wake close to

the turbine, nacelle-based continuous-wave lidars have proven to be suitable [8, 9, 10], whereas long-range pulsed lidars are used to capture the far wake, its propagation path and dispersion [11, 12, 13].
By a combination of multiple lidars the limitation that lidars only measure one-dimensional wind speed information in beam direction can be overcome. A typical way to combine multiple lidars is for example a virtual tower [14, 15, 16]. The WindScanner software developed by the DTU has made an important step towards turbulence measurements with accurately synchronized scanning trajectories [17]. Following the example of Hill *et al.* [18], vertical scans of two lidars are combined in this study to retrieve two-dimensional wind vectors in a vertical plane parallel to the direction of wake propagation. With this approach, the wake propagation and wind speed deficit in stable, near-neutral and convective conditions of the ABL is investigated in a case study of three measurement periods.

2. Experiment description

In the framework of the Perdigão 2017 experiment [19], the German Aerospace Center (DLR) was operating three long-range pulsed Doppler wind lidars of type Leosphere Windcube 200S for dedicated wake measurements of a single 2 MW WEC. Two lidars were placed in-plane with the WEC situated on a mountain ridge which is followed by a valley and a second ridge in a distance of 1.4 km in main wind direction. While one lidar was located in the valley looking up at the WEC, the second lidar was placed on the distant mountain ridge. In this constellation, coplanar measurements allow the retrieval of the two-dimensional wind vector above the valley and, in case of wind directions from south-west, the measurement of wind speed deficit in the wake and its propagation path. For this wind direction, a microwave radiometer is placed upstream to measure the temperature and humidity profile of the incoming flow field. Figure 1 shows an overview of the site. Lidar #1 and lidar #2 are utilized in this study for coplanar vertical scans

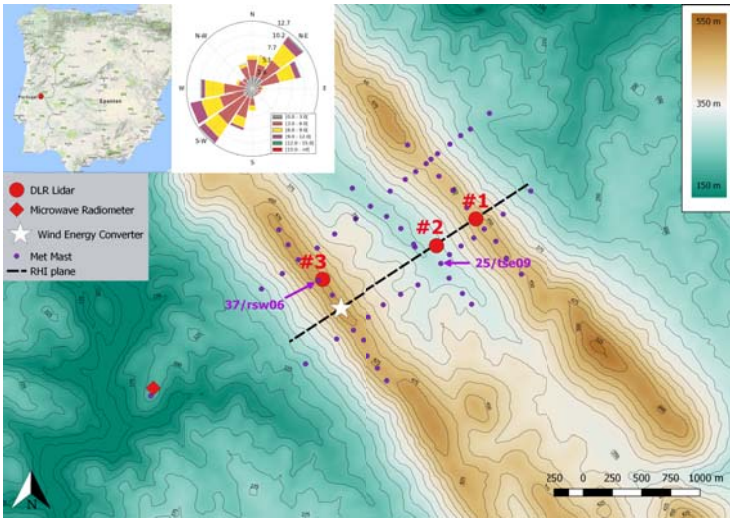

Figure 1. Map of the experimental site with indication of the relevant instrumentation for this study.

in the plane parallel to the main wind direction as indicated by the dashed black line. Lidar #3 is a third DLR instrument, which was placed on the wind turbine ridge to measure the lateral features of the wake, but will not be part of the analysis in this report. Two meteorological masts are used in this analysis: tower $37/rsw06$ is a 60 m mast on the wind turbine ridge which, besides sonic anemometers, is equipped with temperature and humidity sensors on four levels, a

pressure sensor at ground level and can thus be used for the calculation of potential temperature profiles; tower 25/*tse*09 is a 100 m mast in the valley with several sonic anemometers on different levels of which the one at 100 m is used in this study to compare lidar measurements to the in-situ observation and estimate instrument uncertainty. From the intensive operation period

Date	Start	End	Category
9 May 2017	11:00	15:00	convective
11 May 2017	11:00	13:00	neutral
22 May 2017	03:00	07:00	stable

Table 1. List of measurement times (in UTC) for the case study with corresponding stability category.

(IOP) of the experiment which lasted from 1 May to 15 June, three periods have been picked out for this analysis which represent distinct static stability conditions, determined as described in Sect. 3.4 (see Tab. 1).

3. Methods

3.1. Two-dimensional wind vector retrieval

The projection of the wind vector onto a plane can be retrieved from superimposed, coplanar vertical range-height indicator (RHI) scans of two lidars by solving Eq. 1 for horizontal and vertical wind components u and w from line-of-sight wind speeds u_{ri}, where φ_i denote the elevation angles:

$$\begin{bmatrix} u_{\mathrm{r1}} \\ u_{\mathrm{r2}} \end{bmatrix} = \begin{bmatrix} \cos\varphi_1 & \sin\varphi_1 \\ \cos\varphi_2 & \sin\varphi_2 \end{bmatrix} \begin{bmatrix} u \\ w \end{bmatrix} \quad . \tag{1}$$

Parameter	Value
Physical resolution	25 m
Range gate separation	10 m
Angular resolution	0.5° / 1°
Accumulation time	500 ms
Duration of RHI	1-2 min

Table 2. Specifications of lidar settings for RHI scans.

The range gate centers of the single RHI scans do not coincide on the exact same location and same time. Table 2 gives the common parameters of the scans of the two lidars, with the physical resolution being the averaging length along the lidar beam according to [20]. Given the angular resolution of 0.5°, the vertical and horizontal resolution of retrieved measurement points is on the order of 10 m at the WEC hub location. On 22 May, the angular resolution was modified to 1° in order to capture a wider range of elevation in the same time, but this leads to a coarser resolution of approx. 25 m at the WEC hub (see Fig. 5 for an illustration of range gate density). For all cases, the scans of both lidars are linearly interpolated to a common regular grid with a spacing of 10 m and all scans within five-minute intervals are averaged. The resulting grids of measurement points can then be processed with Eq. 1. Figure 2 shows two results of the coplanar retrieval of the two-dimensional flow field for a nighttime stable boundary layer on 22 May 2017. Between 04:00 UTC and 05:00 UTC, the WEC was shut down for one hour, which allows to compare the flow field with and without wake effects. It can be seen that the proposed measurement strategy is well suited to capture the flow field in and above the valley and also allows the detection of the WEC wake.

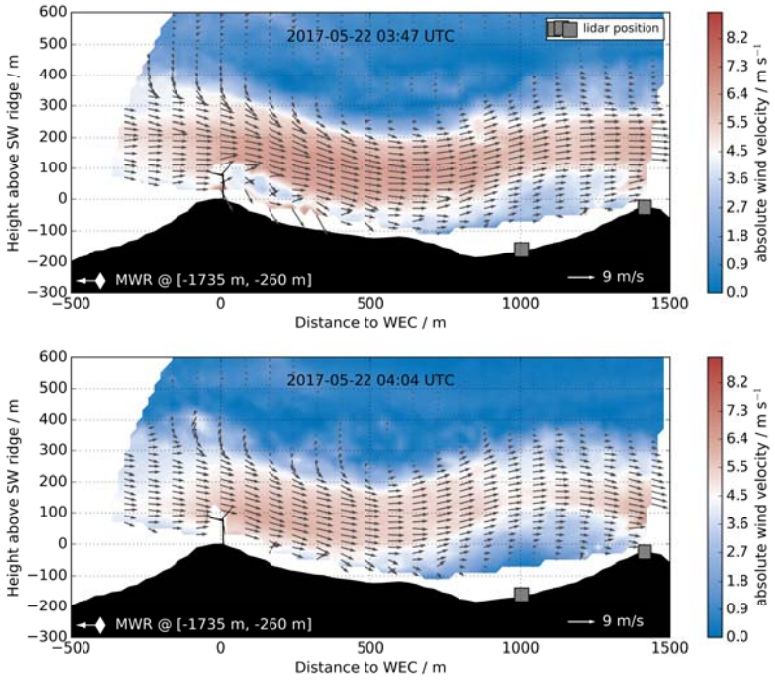

Figure 2. Two five-minute averaged flow field measurements from coplanar scanning lidars. In the upper graph, the WEC wake is clearly visible, in the lower graph the WEC was not operating.

3.2. Uncertainty analysis

The retrieval of both wind vector components in the measurement plane is most solid if the radial wind speed directions are close to perpendicular. The matrix in Eq. 1 becomes singular when both elevation angles are the same, and uncertainties are large if the angles are close to equal. Equations 2-4 give the resulting wind component uncertainties σ_u, σ_w of the Gaussian uncertainty propagation of radial wind speed uncertainties σ_i through Eq. 1 as it has also been used by Hill *et al.* [18].

$$\sigma_u = \frac{1}{|C|}\sqrt{\sin^2\varphi_2\sigma_1^2 - \sin^2\varphi_1\sigma_2^2} \tag{2}$$

$$\sigma_w = \frac{1}{|C|}\sqrt{\cos^2\varphi_1\sigma_2^2 - \cos^2\varphi_2\sigma_1^2} \tag{3}$$

$$C = \sin(\varphi_1 - \varphi_2) \tag{4}$$

Since the elevation angles for both lidars in the Perdigão setup are comparatively small when pointing at the WEC (i.e. $< 20°$), uncertainties of w can become large in the region of the wake. The accuracy of a Windcube 200S is specified with 0.5 m s^{-1} for radial wind speeds [21]. To evaluate the performance in the given experiment, comparative measurements to a sonic anemometer were performed from 15 through 16 June 2017 continuously for 17 hours with fixed stares. The range gate center of the analyzed measurements are horizontally and vertically displaced by approximately 4 m to the anemometer, respectively. The chosen sonic anemometer was at 100 m above ground level on tower #25. Figure 3 shows a regression plot of the lidar radial wind speeds against the projection of the 3D-sonic measurement to the respective lidar beam. The root-mean-squared error (RMSE) of the comparison is close to 0.45 m s^{-1} for both

lidars. While lidar #1 appears to have a constant bias to the sonic anemometer, the error of lidar #2 is changing with increasing wind speeds, showing a larger variance for higher values. It is likely that the observed behaviour is a result of the experimental setup and overestimates the actual instrument errors. Lidar #2 is staring at the sonic anemometer with a higher elevation angle (31°) than lidar #1 (-4°), which means that the vertical wind component is more relevant and could cause the higher variance. Possible reasons are that spatial offsets and the spatial averaging of the lidar are more relevant for the vertical wind components, but even uncertainties in the estimation of vertical wind speeds with sonic anemometers as described by [22] could influence the result. Nevertheless, the value of 0.45 m s^{-1} was used to calculate the uncertainty of the coplanar retrieval for the measurement plane and the result is shown in Fig. 4. The uncertainty of the vertical wind component in the area of interest close to the WEC is too large (> 2.5 m s^{-1}) to be used in the further analysis. Wind speed deficits are therefore calculated using the horizontal wind speeds only of which uncertainties are on the order of the instrument uncertainty.

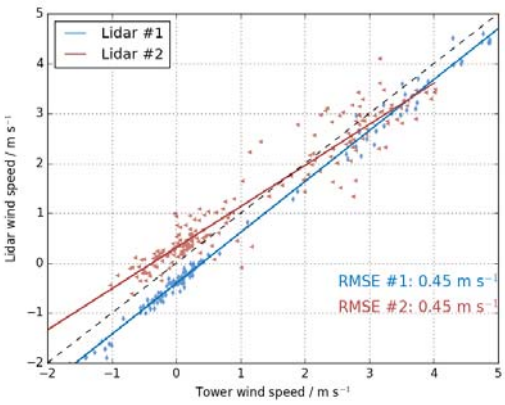

Figure 3. Regression analysis of sonic anemometer on tower 25/*tse*09 and lidar #1 and #2 respectively.

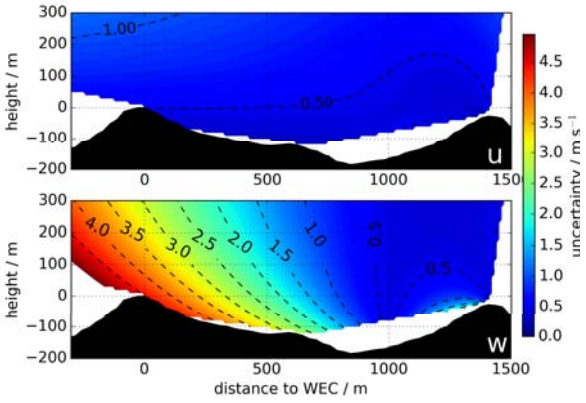

Figure 4. Result of the uncertainty propagation of single lidar uncertainties to the retrieval of a two-dimensional wind vector. The graphs display the uncertainties σ_u of the horizontal (top) and σ_w of the vertical wind component (bottom).

3.3. Wake center tracking algorithm

In order to study the wake propagation in different stability regimes, it is crucial to establish a suitable algorithm to detect and track the wake's center and its widths as it propagates downstream. A similar strategy is used as has been described by [9] and [23] with fits of Gaussian functions to the vertical profiles through the wake. Before applying the Gaussian fit, the profiles are reduced by the logarithmic background profile. It has already been described in [24] that the vertical profile through a wind turbine wake can be simplified to a simple Gaussian function (Eq. 5)

$$u_1(z) = A\, e^{-\frac{(z-b)^2}{2\sigma^2}} + d \tag{5}$$

in the far wake which is the region where rotor shape is less important for the shape of the wake according to [25]. $u_1(z)$ is the function of horizontal wind speeds in dependency of the height z,

A its amplitude, b the maximum position, σ the standard deviation and d an additional offset. In the near wake a superposition of two overlapping Gaussian functions according to

$$u_2(z) = A\left[e^{-\frac{(z-b_1)^2}{2\sigma^2}} + e^{-\frac{(z-b_2)^2}{2\sigma^2}}\right] + d \tag{6}$$

is applicable with σ being the same for both overlapping functions and b_1 and b_2 their individual center position.
Both functions are calculated and a statistical extra sum-of-squares F-test is used according to [23] to decide which function fits the wake shape better and is used to retrieve both wake center and wind speed deficit at each location downstream. The wake tracking is started at 60 m (i.e. 0.75 D) downstream because in closer proximity to the turbine lidar measurements are often corrupted by hard-target hits to the rotor blade. The initial guess of the wake center is set to hub height and is adapted to the actually found wake center for the successive profiles. Figure 5 (left) illustrates how vertical profiles are successively extracted from the gridded wind field and on the right an example of a Gaussian fit to one of the vertical profiles is shown. Tracking of the wake is stopped at the location where no suitable fit to either Eq. 5 or Eq. 6 is possible any more, meaning that one of the following conditions is reached:

- the detected wake center is out of bounds of the vertical profile,
- the amplitude of the fitting function is smaller than 1 m s^{-1} or larger than 20 m s^{-1},
- the standard deviation of the Gaussian function is larger than 2 D,
- or the difference between two succeeding wake center heights is larger than the increment of distances in x-direction (i.e. 10 m).

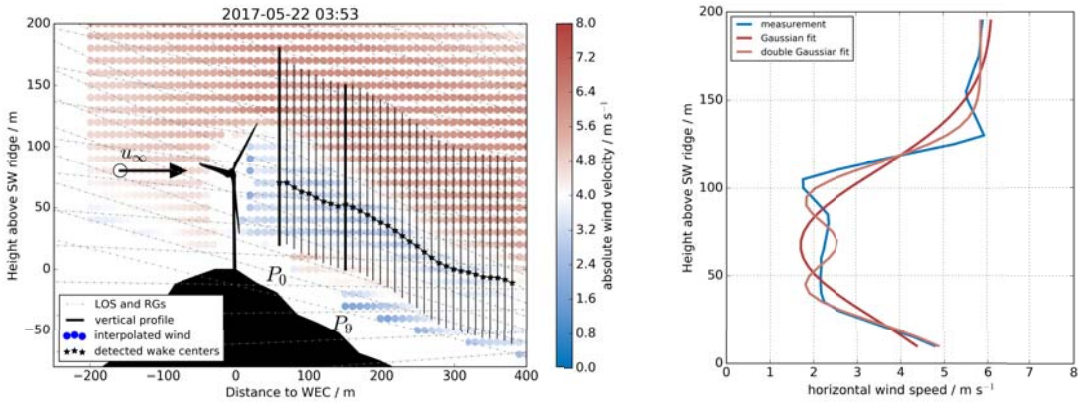

Figure 5. Gridded flow field with indicated vertical profiles for wake detection (left). The thin grey lines and dots show line-of-sight (LOS) lines of the two lidars and the range gate centers (RG). The corresponding vertical profile P_9 with fitted Gaussian functions is shown on the right.

For all detected wakes, the wind speed deficit is calculated as:

$$u_d = 1 - \frac{u(b)}{u_\infty} \tag{7}$$

with $u(b)$ the measured wind speed at the calculated wake center and u_∞ the free stream velocity as measured two rotor diameters upstream by the coplanar retrieval (see Fig. 5). It is evident that even though it is a standard method to define the reference free stream velocity, the streamline and thus the rotor effective wind speed cannot necessarily be traced back to this location in a highly complex flow and large uncertainties are to be expected.

3.4. Static stability estimation

To define the static stability regime, two independent measurements of potential temperature profiles are used. First, microwave radiometer (MWR) measurements that are taken in the far West upstream and second, measurements of in-situ instrumentation on tower 37/rsw06, based on the wind turbine ridge. Figure 6 shows the profiles for the three cases.

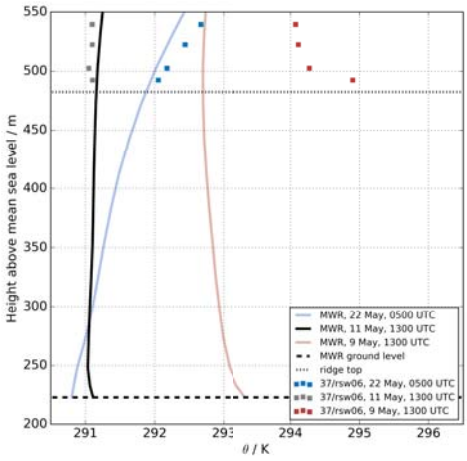

Figure 6. Vertical profiles of potential temperature as measured by the DLR microwave radiometer and meteorological mast 37/rsw06 respectively.

	MWR	37/rsw06
9 May 2017	-0.14 K/100m	-0.11 K/100m
11 May 2017	0.03 K/100m	-0.004 K/100m
22 May 2017	0.21 K/100m	0.62 K/100m

Table 3. Interpolated potential temperature gradient at 50 m above ground level for MWR and tower 37/rsw06.

Both instruments qualitatively agree for the estimation of static stability. The MWR cannot resolve sharp gradients close to the ground appropriately due to its resolution, which leads to a significantly weaker estimation of the inversion in the stable layer as can be read from the values in Tab. 3. The retrieval algorithm of the MWR was also not optimized for the site in Perdigão. In best practice, the retrieval is trained with radiosonde launches at the location of the experiment, which were not available in this case. A retrieval for a location at approximately the same altitude was used instead to guarantee similar ground pressures. The differences in the absolute values of potential temperature, especially in the convective case are likely due to the spatial separation of the instruments and different local surface heating. For the well-mixed near-neutral layer, these differences are not relevant and the measured potential temperatures are almost equal for both measurements.

4. Results and Discussion

The output of the wake tracking algorithm are wake center positions and wind speed deficits in dependency of the distance to the wind turbine for each five-minute averaged flow field. Figure 7 shows the result of the wake center positions for the three periods. While the wake is following the terrain into the valley in stable stratification, it is lifted in the convective case and similarly

so in the near-neutral stratification. Menke *et al.* [26] found similar wake behaviour for this location, but detected more horizontal wake propagation in a near-neutral case. The wake in the stable case can be tracked much further downstream up to at least five rotor diameters and even 10 D for the maximum case. The averages of all five-minute periods are only calculated for distances where at least three single wake cases can be detected. The variance of wake locations in the convective case seems to be larger compared to the near-neutral case, but more data is needed for a solid conclusion. The fact that the first detected wake heights for convective and near-neutral case are at 30 m above hub height in the average is due to the strong vertical component of the flow being accelerated over the ridge, whereas in the stable case the flow follows the terrain. Since near-neutral and convective case appear very similar it can be assumed that static stability is not necessarily the determining factor for the wake propagation path in this complex terrain. Other parameters like Obukhov-length or Richardson number could not be calculated due to a lack of highly-resolved turbulence data. This data will be available in future and allow other classification of wake cases.

The wind speed deficit is plotted over distance to the WEC in Fig. 8. It can be seen that the

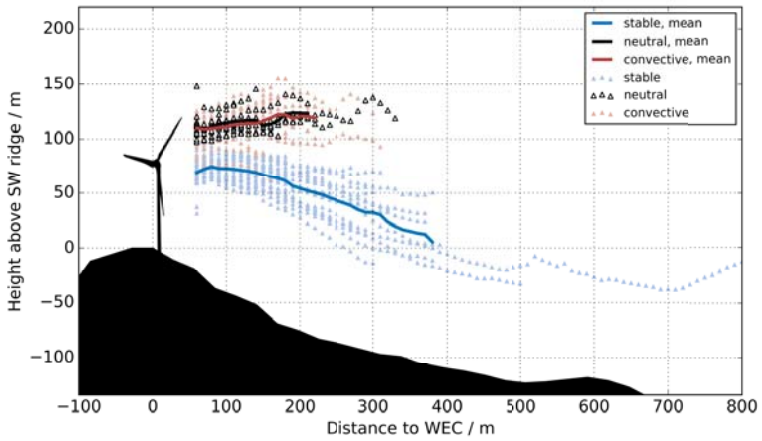

Figure 7. Wake center propagation for three cases of different atmospheric stratification for each single five minute average (dots) and the average for each case (lines).

scatter of single measurements is relatively large, but the mean shows the expected behaviour of decreasing velocity deficit with increasing distance to the WEC and a maximum deficit at approximately 1.5 D. The deficit in the stable case is significantly larger, both in terms of magnitude and length, compared to the neutral and convective cases. The rapid decay of velocity deficit, as seen for convective and neutral stability, is probably due to the strong turbulent mixing in those cases, whereas one wake could be tracked up to 800 m downstream with an almost constant velocity deficit of more than 50% for a stable case, featuring a laminar flow with strongly reduced mixing. Note that the measurement strategy reveals lower bounds of the deficit, as it cannot be guaranteed that the center of the wake with the maximum velocity deficit is captured. Hence, the actual velocity deficits in the wake center might be larger.

Fig. 8 also depicts the temporal evolution of two modelled velocity deficits. Both, the Jensen-Park model [27] and the Frandsen model [28] do not claim to be applicable for non-neutral stratification and complex terrain. They are depicted here nevertheless as reference because they are well known and widely used in both science and industry. For both models a thrust coefficient C_t of 0.72 is used as derived from the theoretical wind speed deficit curve for the WEC in Perdigão according to [29]. A surface roughness length z_0 of 0.5 m for forested area is assumed. It is obvious that the models fail to describe the evolution of the observed deficits.

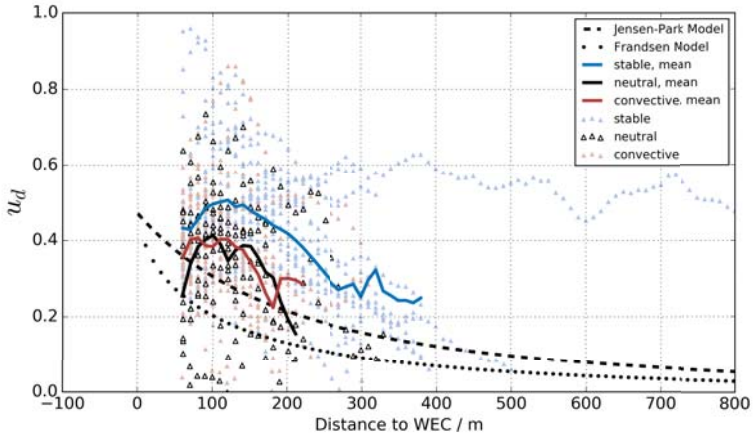

Figure 8. Wind speed deficit u_d in the wake for the three cases. The dashed and the dotted lines show the theoretical wind speed as calculated using the Jensen-Park and the Frandsen model, respectively.

5. Conclusion

Coplanar scans for wake characterization in the Perdigão 2017 experiment are a valuable tool to identify wake propagation for main wind direction and attribute it to different stability regimes. The scans as they were performed do not only measure the flow in the wind turbine wake, but also capture the inflow and the background flow aloft and far downstream which is important for the understanding of the flow in complex terrain in general.

The calculation of wind speed deficits in the wake is problematic with this approach for multiple reasons. First of all, the scanning plane does not always cut the wake at the wake center, which leads to underestimation of the true wind speed deficits. Another problem is of more general nature for complex terrain experiments: the definition of the free-stream velocity. From the retrieved wind field it is obvious that the inflow is strongly influenced by the speed up and flow inclination over the south-west mountain ridge, which means that the wind speed at hub height, two rotor diameters upstream does not necessarily represent the effective inflow. The results of wind speed velocity estimation as it would be done in flat terrain show that the shape and intensity is not well comparable to common engineering models.

Three example cases of wake measurements have been shown in this study to describe the methodology and show the strengths and weaknesses. The Perdigão experiment contains many more periods that are suitable for the presented analysis and will allow to better catagorize wake behaviour to different wind speeds, turbulence intensities, etc. The full potential of the presented measurements can only be exploited in synthesis with microscale modelling of individual cases to understand the processes that lead to the observed wake propagation paths and flow structures.

Acknowledgments

We want to thank José Palma, University of Porto and José Caros Matos and the INEGI team for the local organization and tireless work in order to make this experiment a success. We acknowledge all the hard work of the DTU and NCAR staff to provide large parts of the hardware and software infrastructure available at Perdigão. We appreciate the hospitality and help we received from the municipality of Alvaiade and Vila Velha de Rodão throughout the campaign. This work was performed within projects LIPS and DFWind, both funded by the Federal Ministry of Economy and Energy on the basis of a resolution of the German Bundestag under the contract numbers 0325518 and 0325936A, respectively.

References

[1] Göçmen T, van der Laan P, Réthoré P E, Diaz A P, Larsen G C and Ott S 2016 *Renewable and Sustainable Energy Reviews* **60** 752 – 769 ISSN 1364-0321 URL http://www.sciencedirect.com/science/article/pii/S136403211600143X
[2] Fleming P, Annoni J, Shah J J, Wang L, Ananthan S, Zhang Z, Hutchings K, Wang P, Chen W and Chen L 2017 *Wind Energy Science* **2** 229–239 URL https://www.wind-energ-sci.net/2/229/2017/
[3] Aitken M L, Kosović B, Mirocha J D and Lundquist J K 2014 *Journal of Renewable and Sustainable Energy* **6** 033137 URL https://doi.org/10.1063/1.4885111
[4] Englberger A and Dörnbrack A 2016 *Atmospheric Chemistry and Physics Discussions* **2016** 1–25 URL http://www.atmos-chem-phys-discuss.net/acp-2015-995/
[5] Jimenez A, Crespo A, Migoya E and Garcia J 2007 *Journal of Physics: Conference Series* **75** 012041 URL http://stacks.iop.org/1742-6596/75/i=1/a=012041
[6] Schröttle J, Piotrowski Z, Gerz T, Englberger A and Dörnbrack A 2016 *Journal of Physics: Conference Series* **753** 1–10 URL http://elib.dlr.de/106441/
[7] Wu Y T and Porté-Agel F 2012 *Energies* **5** 5340–5362 ISSN 1996-1073 URL http://www.mdpi.com/1996-1073/5/12/5340
[8] Bingöl F, Mann J and Foussekis D 2009 *Meteorol. Z.* **18** 189–195
[9] Trujillo J J, Bingöl F, Larsen G C, Mann J and Kühn M 2011 *Wind Energy* **14** 61–75 ISSN 1099-1824 URL http://dx.doi.org/10.1002/we.402
[10] Machefaux E, Larsen G C, Troldborg N, Hansen K S, Angelou N, Mikkelsen T and Mann J 2016 *Wind Energy* **19** 1535–1551 ISSN 1099-1824 we.1936 URL http://dx.doi.org/10.1002/we.1936
[11] Iungo G V, Wu Y T and Porté-Agel F 2013 *J. Atmos. Oceanic Technol.* **30** 274–287 URL http://dx.doi.org/10.1175/JTECH-D-12-00051.1
[12] Smalikho I N, Banakh V A, Pichugina Y L, Brewer W A, Banta R M, Lundquist J K and Kelley N D 2013 *J. Atmos. Oceanic Technol.* **30** 2554–2570 URL http://dx.doi.org/10.1175/JTECH-D-12-00108.1
[13] Kumer V M, Reuder J, Svardal B, Sætre C and Eecen P 2015 *Energy Procedia* **80** 245 – 254 ISSN 1876-6102 URL http://www.sciencedirect.com/science/article/pii/S1876610215021608
[14] Calhoun R, Heap R, Princevac M, Newsom R, Fernando H and Ligon D 2006 *J. Appl. Meteorol. Climatol.* **45** 1116–1126 URL http://dx.doi.org/10.1175/JAM2391.1
[15] Newman J F, Klein P M, Wharton S, Sathe A, Bonin T A, Chilson P B and Muschinski A 2016 *Atmospheric Measurement Techniques* **9** 1993–2013 URL http://www.atmos-meas-tech.net/9/1993/2016/
[16] Wang Y, Hocut C M, Hoch S W, Creegan E, Fernando H J S, Whiteman C D, Felton M and Huynh G 2016 *Journal of Applied Remote Sensing* **10** 026015 URL http://dx.doi.org/10.1117/1.JRS.10.026015
[17] Vasiljević N, Lea G, Courtney M, Cariou J P, Mann J and Mikkelsen T 2016 *Remote Sensing* **8** ISSN 2072-4292 URL http://www.mdpi.com/2072-4292/8/11/896
[18] Hill M, Calhoun R, Fernando H J S, Wieser A, Dörnbrack A, Weissmann M, Mayr G and Newsom R 2010 *Journal of the Atmospheric Sciences* **67** 713–729 URL http://dx.doi.org/10.1175/2009JAS3016.1
[19] Mann J, Angelou N, Arnqvist J, Callies D, Cantero E, Arroyo R C, Courtney M, Cuxart J, Dellwik E, Gottschall J, Ivanell S, Kühn P, Lea G, Matos J C, Palma J M L M, Pauscher L, Peña A, Rodrigo J S, Söderberg S, Vasiljevic N and Rodrigues C V 2017 *Philosophical Transactions of the Royal Society of London A: Mathematical, Physical and Engineering Sciences* **375** ISSN 1364-503X URL http://rsta.royalsocietypublishing.org/content/375/2091/20160101
[20] Smalikho I, Köpp F and Rahm S 2005 *Journal of Atmospheric and Oceanic Technology* **22** 1733–1747 URL http://dx.doi.org/10.1175/JTECH1815.1
[21] Leosphere 2016 Windcube 100s/200s/400s weather and climate brochure Tech. rep. Leosphere
[22] Kochendorfer J, Meyers T, Frank J, Massman W and Heuer M 2012 *Boundary-Layer Meteorol.* **145** 383–398 ISSN 0006-8314
[23] Aitken M L, Banta R M, Pichugina Y L and Lundquist J K 2014 *Journal of Atmospheric and Oceanic Technology* **31** 765–787
[24] Ainslie J F 1988 *Journal of Wind Engineering and Industrial Aerodynamics* **27** 213–224
[25] Sanderse B 2009 Aerodynamics of wind turbine wakes - literature review Tech. rep. Energy Research Centre of the Netherlands, ECN-E-09e016
[26] Menke R, Vasiljević N, Hansen K, Hahmann A N and Mann J 2018 *Wind Energy Science Discussions* **2018** 1–18 URL https://www.wind-energ-sci-discuss.net/wes-2018-21/
[27] Jensen N 1983 *A note on wind generator interaction* ISBN 87-550-0971-9
[28] Frandsen S, Barthelmie R, Pryor S, Rathmann O, Larsen S, Højstrup J and Thøgersen M 2006 *Wind Energy* **9** 39–53 ISSN 1099-1824 URL http://dx.doi.org/10.1002/we.189
[29] Menke R 2016 *Investigation of a single wind turbine wake in complex terrain based on Perdigão 2015 multi-LiDAR measurements* Master's thesis Carl von Ossietzky University Oldenburg